Biomass-Derived Nitrogen-Doped Carbon Nanofiber Network: A Facile Template for Decoration of Ultrathin Nickel-Cobalt Layered Double Hydroxide Nanosheets as High-Performance Asymmetric Supercapacitor Electrode

Feili Lai, Yue-E Miao, Lizeng Zuo, Hengyi Lu, Yunpeng Huang, and Tianxi Liu**

The development of biomass-based energy storage devices is an emerging trend to reduce the ever-increasing consumption of non-renewable resources. Here, nitrogen-doped carbonized bacterial cellulose (CBC-N) nanofibers are obtained by one-step carbonization of polyaniline coated bacterial cellulose (BC) nanofibers, which not only display excellent capacitive performance as the supercapacitor electrode, but also act as 3D bio-template for further deposition of ultrathin nickel-cobalt layered double hydroxide (Ni-Co LDH) nanosheets. The as-obtained CBC-N@LDH composite electrodes exhibit significantly enhanced specific capacitance (1949.5 F g^{-1} at a discharge current density of 1 A g^{-1}, based on active materials), high capacitance retention of 54.7% even at a high discharge current density of 10 A g^{-1} and excellent cycling stability of 74.4% retention after 5000 cycles. Furthermore, asymmetric supercapacitors (ASCs) are constructed using CBC-N@LDH composites as positive electrode materials and CBC-N nanofibers as negative electrode materials. By virtue of the intrinsic pseudocapacitive characteristics of CBC-N@LDH composites and 3D nitrogen-doped carbon nanofiber networks, the developed ASC exhibits high energy density of 36.3 Wh kg^{-1} at the power density of 800.2 W kg^{-1}. Therefore, this work presents a novel protocol for the large-scale production of biomass-derived high-performance electrode materials in practical supercapacitor applications.

1. Introduction

The worsening energy crisis and environmental pollution have pushed forward the exploration on high-performance energy storage and conversion systems. Among them, supercapacitors (also called as electrochemical capacitors) have attracted tremendous attention and been widely studied due to their fast charge-discharge rate, high power density, and long-cycle lifetime.[1–3] Typically, supercapacitors can be divided into two types on the basis of their charge storage mechanisms:[4] (i) electric double-layer capacitors (EDLCs), mainly consisting of carbon-based materials, such as carbon nanotubes,[5] graphene,[6] graphene nanoribbon, and carbon nanofibers,[7,8] which possess extraordinary cycling/rate

F. L. Lai, Dr. L. Z. Zuo, Dr. H. Y. Lu,
Dr. Y. P. Huang, Prof. T. X. Liu
State Key Laboratory of Molecular
Engineering of Polymers
Department of Macromolecular Science
Fudan University
Shanghai 200433, P. R. China
E-mail: txliu@fudan.edu.cn

Dr. Y.-E. Miao, Prof. T. X. Liu
State Key Laboratory for Modification
of Chemical Fibers and Polymer Materials
College of Materials Science and Engineering
Donghua University
Shanghai 201620, P. R. China
E-mail: yuee_miao@dhu.edu.cn

DOI: 10.1002/smll.201600412

stability but low specific capacitance; (ii) pesudocapacitors, mainly made up of metal oxides/hydroxides and conductive polymers, such as Co_3O_4, MnO_2, $Ni(OH)_2$, and polyaniline,[9,10] which generally possess high specific capacitance/energy density but poor stability. Among various pseudocapacitive electrode materials, nickel-cobalt layered double hydroxide (Ni-Co LDH) with a chemical formula of $[M^{2+}{}_{1-x}M^{3+}{}_x(OH)_2]x^+[An^-{}_{x/n}\cdot mH_2O]x^-$ (where M^{2+} is a divalent metal cation, M^{3+} is a trivalent metal cation and An^- is the interlayer anion) is one of the most promising candidates for high-performance supercapacitors,[11–14] attributing to its unique lamellar structure with large interlayer spacing for enhanced anion exchange properties.[15] Xu et al. reported the novel construction of hierarchical $NiCoO_2$ nanosheets nanotubes via a mild solution method by using polymeric nanotubes as the template,[16] delivering a high specific capacitance of 1468 F g^{-1} at the discharge current density of 2 A g^{-1}. Meanwhile, template-free Ni-Co LDH nanoflowers with controllable sizes were also synthesized as potential electrode materials for pesudocapacitors.[17] However, the reported capacities of pure nickel-cobalt hydroxides are still confined by their limited active sites for effective electrochemical reactions which results from the severe agglomeration of Ni-Co LDH nanoparticles. In addition, due to the low electrical conductivity of inorganic materials, the electron-transfer process is restrictedly localized near the surface of Ni-Co LDH nanoparticles which obviously limits the improvement of electrochemical property. In order to maximize the intrinsic properties of nickel-cobalt layered double hydroxides, it is vital to design Ni-Co LDH based electrode materials with hierarchical structures and multiple pathways for effective ion/electron transfer.

Coincidentally, the hybridization of Ni-Co LDH/$NiCo_2O_4$ with carbon-based materials has been regarded as a simple but effective strategy to obtain composite materials that simultaneously exhibit outstanding EDLC and pseudocapacitive performances, such as multi-walled carbon nanotube/nickel-cobalt binary metal hydroxide composites,[18] nickel cobalt oxide/reduced graphene oxide composite materials,[19,20] cobalt and nickel double hydroxide nanosheets/porous $NiCo_2O_4$ nanowires/carbon fiber paper,[21] cobalt-nickel LDH nanoflakes/carbon fibers.[22] Recently, Lou et al. successfully synthesized $NiCo_2O_4$ nanorods/ultrathin nanosheets on carbon nanofibers to form an excellent electrode material with high power and energy densities, which is ascribed to its high electroactive surface area and porous feature,[23] indicating the virtues of continuous carbon nanofibers as a template for immobilization of metal oxides/hydroxides. Compared with synthetic carbon nanofibers (such as polyacrylonitrile-based carbon nanofibers, polyimide-based carbon nanofibers, and ordered mesoporous carbon nanofibers),[24–26] biomass-derived carbon nanofibers have been considered as a more promising candidate for next-generation electrochemical electrode materials owning to their abundant resource, low cost, easy fabrication, and eco-friendliness.[27–29] Bacterial cellulose is one kind of typical biomass precursors with 3D networks consisting of superfine nanofibers (≈50 nm in diameter), which is produced through microbial fermentation.[30] Chen et al. fabricated a binder-free asymmetric supercapacitor using MnO_2 nanosheets decorated carbon nanofibers deriving from bacterial cellulose as electrode materials, which surprisingly delivers high energy density and power density.[31] Similarly, Ni_3S_2/carbon nanofiber composites derived from bacterial cellulose via a hydrothermal method also present excellent specific capacitance and good cycle stability.[32] In addition, the introduction of heteroatoms (such as nitrogen atom) into carbocyclic rings can adjust the valence orbital energy levels of the surface carbon to provide more electron transfer pathways, leading to largely improved electrochemical performance.[33–37]

Here, we prepared a novel composite of nitrogen-doped carbonized bacterial cellulose@nickel-cobalt layered double hydroxide (CBC-N@LDH) with hierarchical structures via undergoing in situ oxidative polymerization, high-temperature carbonization and solution co-deposition processes consecutively (**Figure 1**a). This CBC-N@LDH composite displays an enhanced specific capacitance of 1949.5 F g^{-1} at a discharge current density of 1 A g^{-1} (based on active materials), a high capacitance retention of 54.7% even at a high discharge current density of 10 A g^{-1}, and excellent cycling stability of 74.4% retention after 5000 cycles, which is because of the uniform dispersion of ultrathin hydrotalcite-like Ni-Co LDH on the surface of nitrogen-doped carbon nanofibers, the intimate contact between CBC-N nanofibers and Ni-Co LDH nanosheets, and the highly conductive 3D network consisting of nitrogen-doped carbon nanofibers. Moreover, the asymmetric supercapacitor, with CBC-N@LDH composites as positive electrode materials and CBC-N nanofibers as negative electrode materials, exhibits wide potential window of 0–1.6 V and high energy density of 36.3 Wh kg^{-1} at a power density of 800.2 W kg^{-1}, demonstrating its potential applications in high-performance energy storage devices.

2. Results and Discussion

The hydrogel consisting of bacterial cellulose nanofibers (Figure 1b) was cut into rectangular squares with the size of 4 × 5 cm^2 and freeze-dried to obtain spumescent bacterial cellulose aerogel (as shown in the inset of Figure 1b). In Figure 1c, carbonized bacterial cellulose (CBC) aerogel (inset in Figure 1c) shows a 3D network structure consisting of numerous intertwined carbon nanofibers with diameter of 30-60 nm. This unique structure is an ideal template for growth of polyaniline, which can significantly minimize the severe aggregation of pure PANI particles (Figure 1d). For CBC-N1 nanofibers (Figure 1e), only sparsely distributed PANI nanoparticles are observed among the carbon nanofiber networks. With the increase of ANI amount, uniform PANI coating is achieved for CBC-N2 nanofibers (Figure 1f) with diameter of ≈200 nm to form uniform core-sheath nanostructure, which is attributed to the strong hydrogen bonding between the rich hydroxyl groups of bacterial cellulose nanofibers and amine groups of aniline.[38] Moreover, the well-reserved 3D porous network nanostructure of CBC-N2 nanofibers is beneficial to the ion diffusion into the inner space for further growth of nickel-cobalt layered double hydroxides on the coarse surface

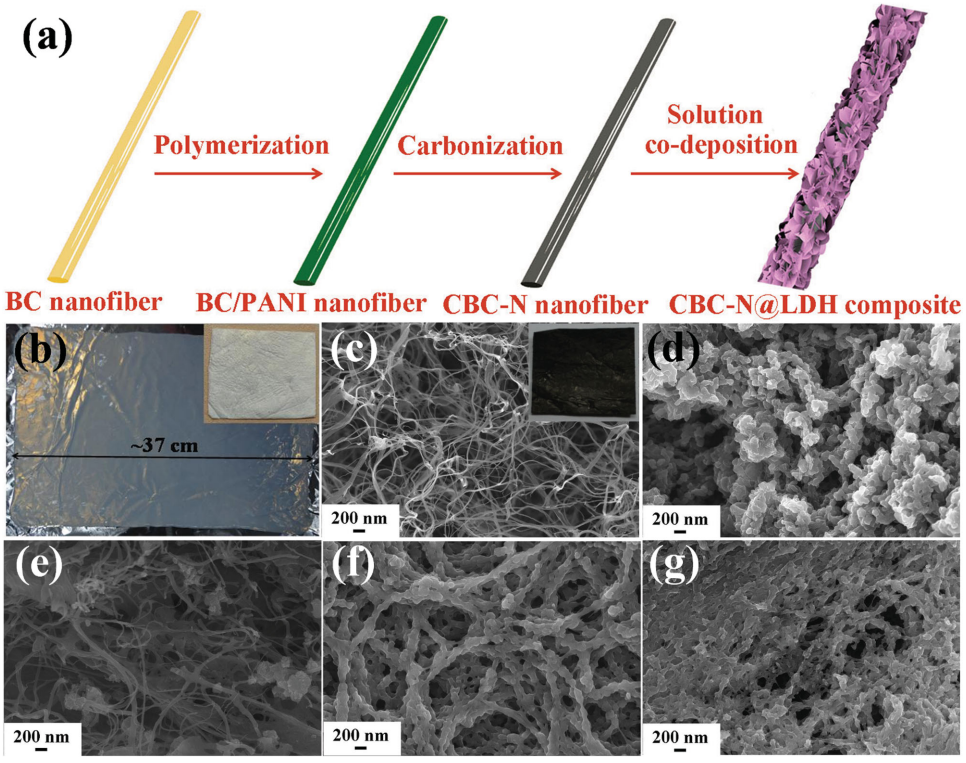

Figure 1. a) Schematic for the preparation of CBC-N@LDH composites; b) Photographs of the pristine bacterial cellulose pellicle and freezing-dried bacterial cellulose membrane (inset) with size of 30 × 40 cm^2 and 4 × 5 cm^2, respectively; c) FESEM image and photograph (inset) of CBC membrane; FESEM image of pure d) PANI powder, e) CBC-N1, f) CBC-N2, and g) CBC-N3 nanofibers.

of nanofibers through solution co-deposition method. However, when the amount of ANI monomer is further increased, excessive growth of PANI with buried carbon nanofibers emerges as shown in Figure 1g, which would severely impede the ion diffusion process. Therefore, CBC-N2 nanofibers are considered as the ideal nitrogen-doped carbon materials with good preservation of 3D interconnected networks and appropriate coverage of carbonized polyaniline layer.

For further construction of high-performance electrode materials, ultrathin nickel-cobalt layered double hydroxide nanosheets are deposited on the surface of CBC-N2 nanofibers through a facile solution co-deposition process. As shown in **Figure 2**a, the sparse distribution of Ni-Co LDH nanosheets on the surface of CBC-N2 nanofibers for CBC-N2@LDH-0.1 composite is because of the lack of Ni^{2+} and Co^{2+} sources in the mixed solution. The appropriate concentration of Ni^{2+} sources is fixed at 0.4 mmol for CBC-N2@LDH-0.4 composite (Figure 2b), where porous structure consisting of continuous CBC-N2@LDH-0.4 nanofibers with an increased diameter to about 600 nm is well maintained even after the growth of Ni-Co LDH nanosheets. The magnified image in the inset of Figure 2b and TEM images in Figure S3 (Supporting Information) further confirms that ultrathin Ni-Co LDH nanosheets are uniformly anchored on the surface of nitrogen-doped carbon nanofibers to form hierarchical core-shell structure compared with the severe aggregation of pure Ni-Co LDH nanoparticles (Figure S1, Supporting Information), which is beneficial to drastically increase the exposed electroactive sites for

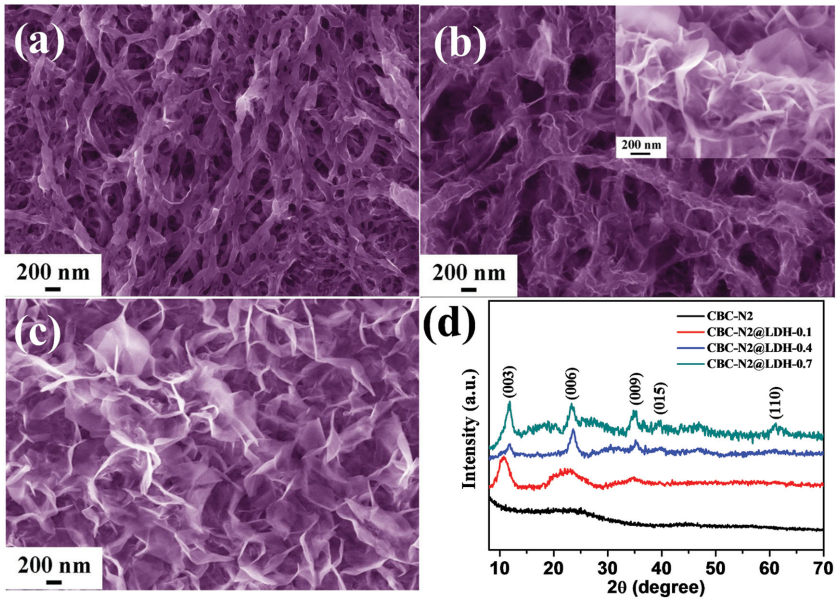

Figure 2. FESEM images of a) CBC-N2@LDH-0.1, b) CBC-N2@LDH-0.4, and c) CBC-N2@LDH-0.7 composites. d) X-ray diffraction patterns of CBC-N2 nanofibers, CBC-N2@LDH-0.1, CBC-N2@LDH-0.4, and CBC-N2@LDH-0.7 composites.

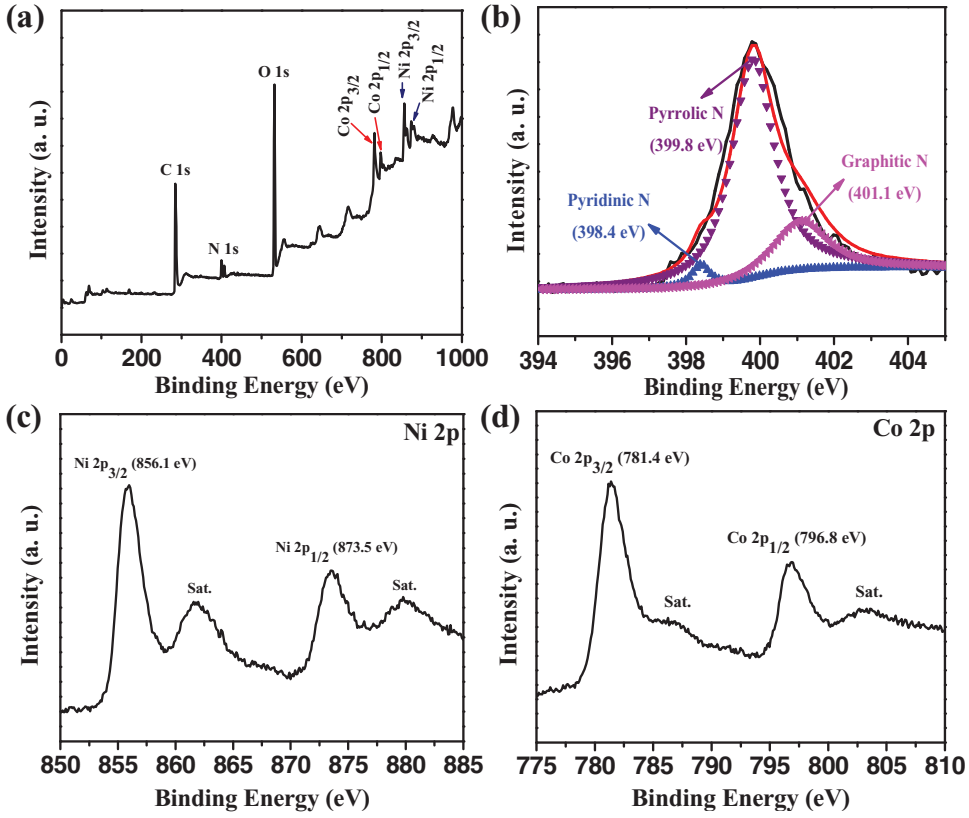

Figure 3. XPS spectra of CBC-N2@LDH-0.4 composite: a) the full survey scan, b) N 1s, c) Ni 2p, and d) Co 2p.

enhanced oxidation/reduction reactions between nickel-cobalt layered double hydroxides and OH^-, and to accelerate the electron transport rate among ultrathin nanosheets by incorporating highly conductive nitrogen-doped carbon nanofibers. The corresponding energy dispersive spectrum further demonstrates the elementary composition of Ni, Co, C, and O in CBC-N2@LDH-0.4 composite (Figure S2, Supporting Information). An increased dosage of Ni-Co LDH precursor is also investigated. However, CBC-N2 nanofibers are totally buried by the excessive deposition of Ni-Co LDH nanosheets, leading to clogged 3D porous structure of CBC-N2@LDH-0.7 composite (Figure 2c). Additionally, Brunauer-Emmett-Teller (BET) analysis of CBC-N2@LDH-0.4 composite (Figure S4, Supporting Information) shows a high specific surface area of 405.8 $m^2\ g^{-1}$ and a narrow pore size distribution in the range of 1-10 nm, which can be attributed to the natural porous structure of bacterial cellulose and the hierarchical core-shell structure of CBC-N2@LDH-0.4 composite.

The structures of various samples were recorded by XRD and XPS tests. As previously reported,[39] bacterial cellulose possesses three sharp peaks at 2θ = 15.0°, 17.4°, and 23.3° (black line in Figure S5, Supporting Information), which can be assigned to the $(1\bar{1}0)$, (110) and (020) planes respectively, indicating its typical cellulose I allomorph structure with high crystallinity.[40] After carbonization of BC/PANI, amorphous nitrogen-doped carbon nanofibers are obtained with two broad peaks at 2θ = 25.1° and 45.1° (Figure 2d), which is similar to the amorphous CBC nanofibers (red line in Figure S5, Supporting Information). Importantly, the well-defined diffraction peaks observed at 2θ = 11.7°, 23.3°, 35.0°, 39.4°, and 60.5° for CBC-N2@LDH composite (Figure 2d) can be indexed to the (003), (006), (009), (015), and (110) planes of hydrotalcite-like LDH phase.[11] The unique hydrotalcite-like structure is undoubtedly in favor of fast ion diffusion among the enlarged interlayer space of layered double hydroxides. As shown in **Figure 3**a, the XPS spectrum of CBC-N2@LDH-0.4 composite exhibits five peaks centered at the C, O, N, Co, and Ni core-level regions, which can be assigned to C 1 s, O 1 s, N 1s, Co 2p, and Ni 2p, respectively. The nitrogen atom is successfully incorporated into carbon nanofibers, with three well-fitted peaks centered at 398.4, 399.8, and 401.1 eV (Figure 3b) corresponding to the pyridinic-like, pyrrolic-like, and graphitic-like nitrogens, respectively.[41] As displayed in the Ni 2p spectrum (Figure 3c), two spin-orbit doublets centered at 856.1 and 873.5 eV accompanied with two shake-up satellites are identified as Ni $2p_{3/2}$ and Ni $2p_{1/2}$ respectively, demonstrating the successful achievement of Ni^{2+}. In analogy to Ni element, the peaks situated at 781.4 eV and 874.0 eV with two pretty weak shake-up satellites are assigned to Co $2p_{3/2}$ and $2p_{1/2}$ atomic orbitals, which indicates the co-existence of Co^{2+} and Co^{3+}.[42] In order to investigate the mass loading of active materials (refer to Ni-Co LDH nanosheets) in various CBC-N2@LDH composites, TGA curves are shown in Figure S6 (Supporting Information). Table S1 (Supporting Information) shows that the mass loading of Ni-Co LDH nanosheets are 15.6%, 19.9%, and 34.3% for CBC-N2@LDH-0.1, CBC-N2@LDH-0.4, and CBC-N2@LDH-0.7 composites, respectively. Further detailed analysis for TGA curves and the corresponding calculating process are appended in Supporting Information.

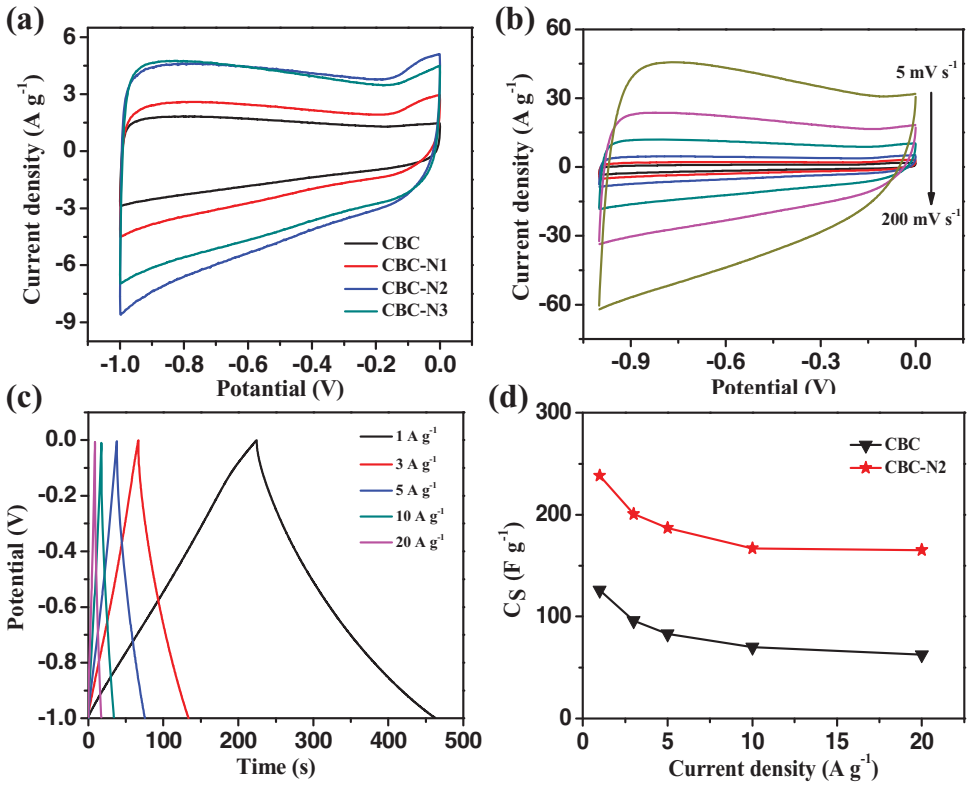

Figure 4. a) CV curves of CBC, CBC-N1, CBC-N2, and CBC-N3 nanofibers at a scan rate of 20 mV s^{-1}; b) CV curves of CBC-N2 nanofibers at various scan rates; c) Galvanostatic charge-discharge curves at various current densities for CBC-N2 nanofibers; d) Specific capacitance of CBC-N2 and CBC nanofibers at various current densities.

The obtained nitrogen-doped carbon nanofibers and CBC-N2@LDH composites were respectively assembled as the negative and positive electrode materials for supercapacitor applications. As shown in **Figure 4**a, CV curves of various carbon nanofiber electrodes (i.e., CBC, CBC-N1, CBC-N2, and CBC-N3) display near-rectangular shapes at a scan rate of 20 mV s^{-1}, demonstrating the ideal double-layer capacitance behavior based on enhanced ion diffusion/adsorption processes. Compared with bacterial cellulose-derived carbon nanofibers, nitrogen-doped carbon nanofiber electrodes exhibit much higher capacitive performance due to more abundant active sites for electric double-layer formation and Faradic redox reactions which result from the effective nitrogen doping.[43] Among various nitrogen-doped carbon nanofiber electrodes, CBC-N2 nanofiber electrode shows the most excellent capacitive performance, which can be attributed to the more rich nitrogen doping and well-maintained 3D porous structure originating from bacterial cellulose. Linear and symmetrical galvanostatic charge-discharge curves of CBC-N2 nanofibers at various current densities are shown in Figure 4c, exhibiting a high specific capacitance of 238.4 F g^{-1} at a current density of 0.5 A g^{-1}, which is comparable with many other carbon-based electrode materials, such as hierarchical porous carbons (214 F g^{-1} at a scan rate of 5 mV s^{-1}),[44] and metal-organic framework-derived carbons (251 F g^{-1} at a scan rate of 5 mV s^{-1}).[45] In addition, the rate stability is another significant criterion for carbon-based electrode materials, which is reflected in Figure 4b with good shape preservation of the CV curve for CBC-N2 nanofibers even at a high scan rate of 200 mV s^{-1}. As shown in Figure 4d, a higher rate capability retention (69.3%) for CBC-N2 electrode materials is observed compared with that (49.7%) of CBC electrode materials without nitrogen doping at the maximal discharge current density of 20 A g^{-1}. The excellent cycling stability of above 95% retention after 2000 cycles (Figure S7, Supporting Information) further indicates nitrogen-doped carbon nanofibers are expected to be one kind of possible alternatives of the existing carbon-based electrode materials for energy storage applications.

The specific capacitances of various CBC-N@LDH composite electrodes are also investigated via a three-electrode system. As shown in **Figure 5**a, a pair of redox peaks with cathodic peaks at about 0.12 V and anodic peaks around 0.23 V are observed for all CBC-N2@LDH composite electrodes when the scan rate is 5 mV s^{-1}, indicating their good pseudocapacitive characteristics arising from the Faradaic redox reactions of M-O-OH (where M refers to Ni or Co). As the capacitance is directly proportional to the area of CV curves, the CBC-N2@LDH-0.4 composite is deduced to show the maximum capacitance, which can be associated with the appropriate growth of nickel-cobalt layered double hydroxides on the surface of nitrogen-doped carbon nanofibers to provide abundant pores for electrolyte penetration and more electroactive sites for electrochemical reaction. Furthermore, its significantly increased property than that of pure Ni-Co LDH powder also proves that it is an efficient strategy to enhance the specific capacitance of pseudocapacitive materials by immobilizing them on the surface of nitrogen-doped

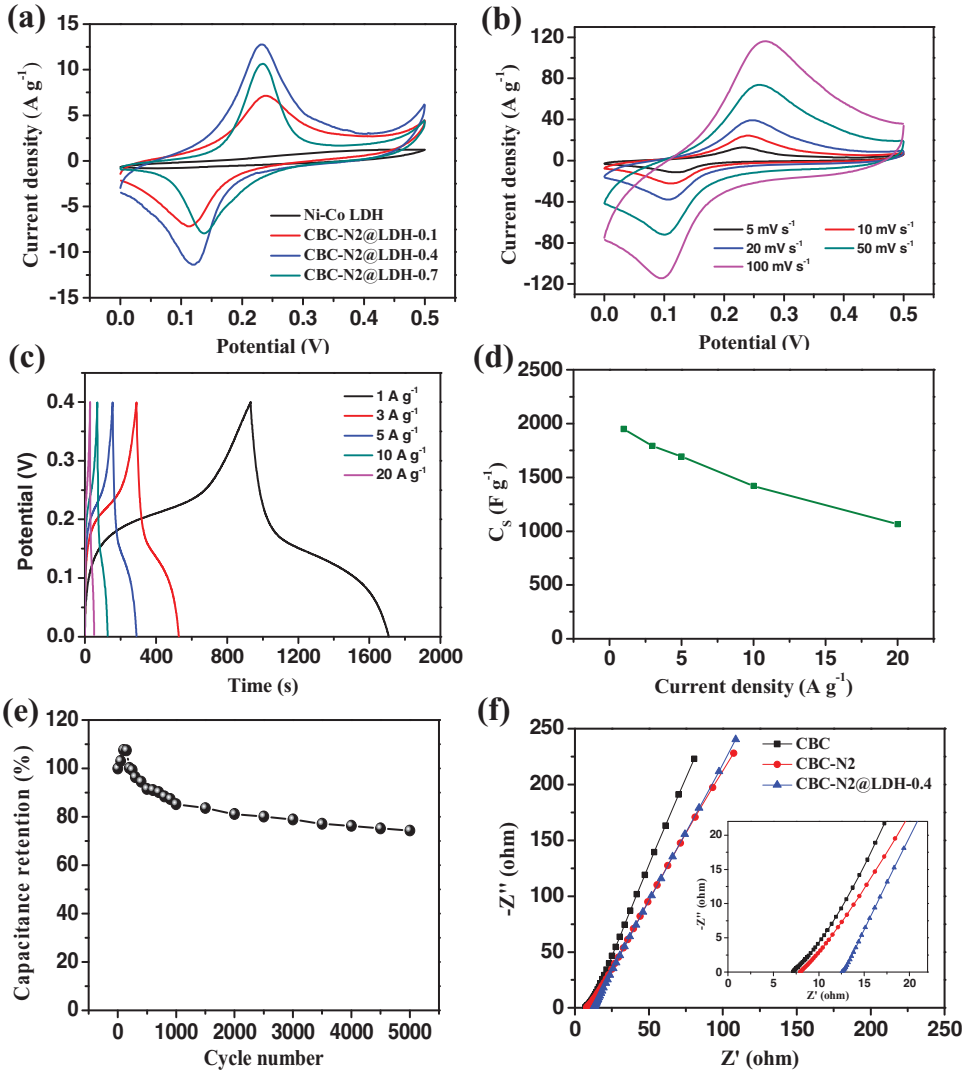

Figure 5. a) CV curves of Ni-Co LDH powders, CBC-N2@LDH-0.1, CBC-N2@LDH-0.4, and CBC-N2@LDH-0.7 composites at a scan rate of 5 mV s^{-1}; b) CV curves of CBC-N2@LDH-0.4 composite at various scan rates; c) Galvanostatic charge-discharge curves at various current densities for CBC-N2@LDH-0.4 composite; d) Specific capacitance of CBC-N2@LDH-0.4 composite at various current densities; e) The long-term cycling performance of CBC-N2@LDH-0.4 composite at a scan rate of 100 mV s^{-1}; f) Nyquist plots of CBC, CBC-N2, and CBC-N2@LDH-0.4 based electrode materials.

carbon materials. To further explore the electrochemical performance of CBC-N2@LDH-0.4 composite, CV curves at various scan rates are recorded in Figure 5b. With a 20-fold increase in the scan rate from 5 to 100 mV s^{-1}, only slight shift of the anodic peak from 0.233 to 0.269 V is observed, indicating the low resistance of the electrode material because of the highly conductive CBC-N2 nanofibers and its good contact with ultrathin Ni-Co LDH nanosheets. In addition, the symmetric shapes and voltage plateaus at 0.15–0.2 V in the galvanostatic charge-discharge curves of CBC-N2@LDH-0.4 composite in Figure 5c, reveal its typical pseudocapacitive behaviors as well. The calculated specific capacitance through Equation (3) is 1949.5 F g^{-1} at a discharge current density of 1 A g^{-1} (based on the active materials), which is considerably higher than those of most previously reported values on nickel-cobalt oxides/hydroxides (Table S2, Supporting Information). Furthermore, even at a high current density of 20 A g^{-1}, 54.7% of the capacitance (1066.0 F g^{-1}) is still retained for the CBC-N2@LDH-0.4 composite (Figure 5d), which probably results from the uniform distribution of Ni-Co LDH nanosheets on the surface of nitrogen-doped carbon nanofibers and thus generated 3D networks for enhanced penetration of OH^-. The cycling life performance is obtained in alkaline solution with a scan rate of 100 mV s^{-1} (Figure 5e). Interestingly, the specific capacitance of CBC-N2@LDH-0.4 composite increases firstly and decays slightly after 100 cycles. Due to the merits of the nitrogen-doped carbon nanofiber template, CBC-N2@LDH-0.4 composite still remains high capacitance retention of 74.4% after 5000 cycles, demonstrating its good conductivity and excellent cycling stability, which can be further demonstrated by the almost overlapped impedance plots before and after 5000 cycles (Figure S8, Supporting Information). Figure 5f compares the Nyquist plots of CBC, CBC-N2, and CBC-N2@LDH-0.4 composites at the open-circuit potential in the frequency range from 100 kHz to 0.01 Hz. No obvious semicircle is observed for all of the above electrodes in the high-frequency region, which is attributed to the high charge

small NANO MICRO

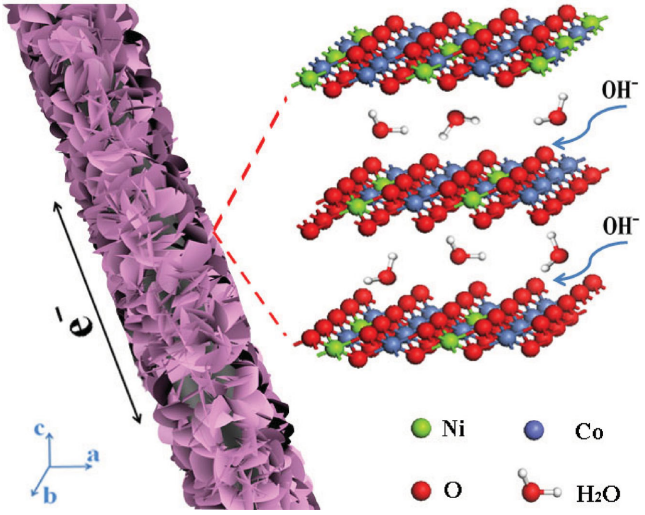

Figure 6. Illustration of the electrochemical processes for CBC-N@LDH composite.

transfer process. Furthermore, the vertical slopes in the low-frequency region correspondingly indicate their low ion diffusion and electron transfer resistance.

In conclusion, the enhanced electrochemical performance of CBC-N@LDH composites can be mainly ascribed to four reasons: First, the uniform dispersion of ultrathin nickel-cobalt layered double hydroxide nanosheets on the surface of nitrogen-doped carbon nanofibers can obviously increase their specific surface area and efficiently enlarge the contact area between the electrode materials and electrolyte. Second, as shown in **Figure 6**, the unique hydrotalcite-like structure of Ni-Co LDH is beneficial to the penetration of OH^- even into the inner spaces between two atomic layers of layer double hydroxides, which can dramatically enlarge their contact area, and promote the following Faradaic reactions of $Ni_xCo_y(OH)_z$[46]:

$$Ni_x\,Co_y\,(OH)_z + OH^- \leftrightarrow NiOOH + CoOOH + H_2O + e^- \quad (1)$$

$$CoOOH + OH^- \leftrightarrow CoO_2 + H_2O + e^- \quad (2)$$

Third, the generated electrons from Equations (1) and (2) can first transfer during the atomic layers of Ni-Co LDH (Figure S9, Supporting Information), and then pass on to the highly conductive nitrogen-doped carbon nanofibers due to the close contact between CBC-N nanofibers and Ni-Co LDH nanosheets. Fourth, by the merits of the as-formed 3D networks, electrons can transfer among the inner structures of the electrode rapidly and directly. Therefore, this contrivable structure of CBC-N@LDH composites with easy-fabrication processes puts forward a novel strategy for the design and fabrication of hierarchically structured composite electrode materials combining excellent electric double-layer capacitance and pseudocapacitance.

Then, an asymmetric supercapacitor (ASC) was assembled using CBC-N2@LDH-0.4 composite as the positive electrode material and CBC-N2 nanofibers as the negative electrode material as illustrated in **Figure 7**a, which was assigned as CBC-N2@LDH-0.4//CBC-N2. Attributing to the collective contribution of electric double-layer capacitance and pseudocapacitance, a wider potential window from 0 to 1.6 V is applied for CBC-N2@LDH-0.4//CBC-N2 as shown in Figure 7b. The CV shape is well retained, even at a high scan rate of 200 mV s^{-1}, indicating the fast charge-discharge properties of the device. The galvanostatic charge-discharge curves collected at different current densities are shown in Figure 7c, with the symmetric triangular shapes revealing its rapid I-V response. Moreover, the rapid I-V response can further be verified from the small variation of the IR drop (IR_{drop}) at different discharge current densities (Figure S10, Supporting Information) ($IR_{drop}[V] = 0.0033 + 0.012\frac{I}{M}[A\ g^{-1}]$), which favors a high discharge power delivery to meet practical applications. According to Equation (3), the specific capacitances based on the total mass are calculated to be 101.9, 95.6, 90.9, 73, and 63.8 F g^{-1} for the as-assembled ASC device at current densities of 1, 2, 3, 5, and 10 A g^{-1} respectively (Figure 7d). A high capacitance retention of 62.6% is observed even at a high current density of 10 A g^{-1}, which is closely related with the unique 3D structure constructed by nitrogen-doped carbon nanofibers and nickel-cobalt layered double hydroxides nanosheets. Moreover, the energy and power densities are also calculated from the galvanostatic discharge curves (based on Equations (4) and (5)) and plotted on the Ragone diagram. As shown in Figure 7e, the as-assembled CBC-N2@LDH-0.4//CBC-N2 ASC device shows a maximum energy density of 36.3 Wh kg^{-1} at the power density of 800.2 W kg^{-1} and a high power density of 8000 W kg^{-1} at the energy density of 22.7 Wh kg^{-1}. The result is higher than those of other previously reported values, such as Ni-Co hydroxide/graphene/nickel foam//activated carbon (20.84 Wh kg^{-1} at a power density of 7500 W kg^{-1}),[47] $Ni_{0.32}Co_{0.68}(OH)_2$//graphene oxide (33 Wh kg^{-1} at a power density of 970 W kg^{-1}),[48] nickel-cobalt hydroxide nanoflowers//activated carbon (20.6 Wh kg^{-1} at a power density of 3930 W kg^{-1}),[17] nickel-cobalt hydroxides//activated carbon (19.1 Wh kg^{-1} at a power density of 7000 W kg^{-1}),[49] and Ni_xCo_{1-x} LDH-Zn_2SnO_4//activated carbon (23.7 Wh kg^{-1} at a power density of 284.2 W kg^{-1}).[50] Meanwhile, the EIS experiment of the asymmetric supercapacitor was carried out to further investigate its electrochemical behavior with rapid electron-transfer and diffusion processes during charge-discharge reaction (Figure S11, Supporting Information). Furthermore, the durability of the as-assembled ASC device was also evaluated. After 2500 cycles, the ASC device still keeps a high capacitance retention of 89.3% (Figure 7f), which is comparable to those of other ASC devices.[47] The above performance indicates that the CBC-N2@LDH-0.4 and CBC-N2 electrodes are both promising candidates for the next-generation energy storage applications.

3. Conclusion

In summary, nitrogen-doped carbon nanofibers were obtained by directly carbonizing polyaniline-coated bacterial cellulose nanofibers, showing a high specific capacitance of 238.4 F g^{-1}

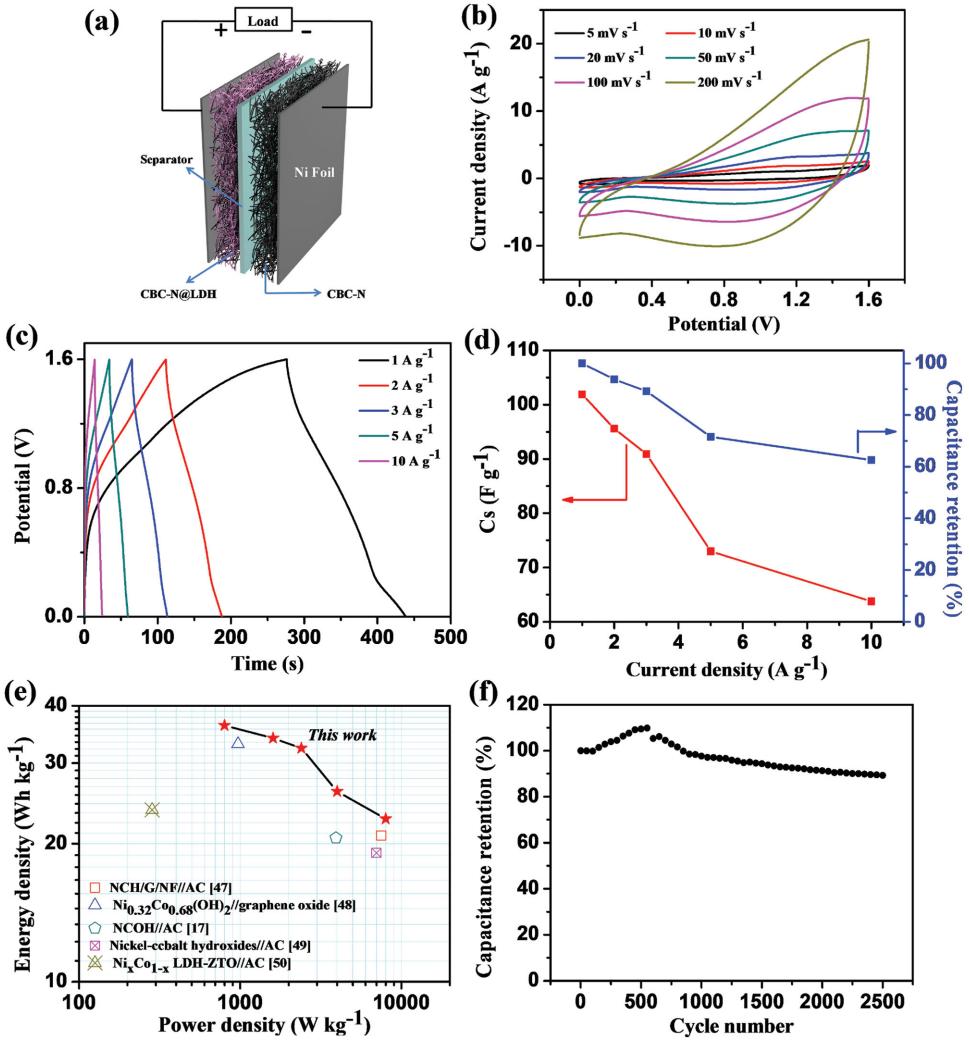

Figure 7. a) Schematic of the assembled structure of an asymmetric supercapacitor based on CBC-N2@LDH-0.4 composite as the positive electrode material and CBC-N2 nanofibers as the negative electrode material; b) CV curves at various scan rates and c) galvanostatic charge-discharge curves at various current densities for the assembled asymmetric supercapacitor; d) Specific capacitance and the corresponding capacitance retention of the as-assemble CBC-N2@LDH-0.4//CBC-N2 ASC device at different current densities; e) Ragone plots of the as-assembled ASC device and recently reported values for comparison (Here, NCH, G, NF, AC, NCOH, and ZTO are denoted as Ni-Co hydroxide, graphene, nickel foam, activated carbon, nickel cobalt hydroxide nanoflowers, and Zn_2SnO_4, respectively); f) The long-term cycling performance of the device at a scan rate of 100 mV s^{-1}.

at a current density of 0.5 A g^{-1}. Moreover, nickel-cobalt layered double hydroxide nanosheets can be easily anchored on the surface of nitrogen-doped carbon nanofibers by a simple solution co-deposition process to form CBC-N@LDH composites with hierarchical structures. The uniform distribution of ultrathin hydrotalcite-like Ni-Co LDH nanosheets, the intimate contact between CBC-N nanofibers and Ni-Co LDH nanosheets, and highly conductive 3D networks consisting of nitrogen-doped carbon nanofibers jointly lead to the excellent capacitive performance with a significantly enhanced specific capacitance of 1949.5 F g^{-1} at a discharge current density of 1 A g^{-1} (based on active materials), a high capacitance retention of 54.7% even at a high discharge current density of 10 A g^{-1} and excellent cycling stability of 74.4% retention after 5000 cycles. The asymmetric supercapacitor assembled by using CBC-N@LDH composite as the positive electrode material and CBC-N nanofibers as negative electrode material, can be operated under a wide potential window of 0-1.6 V with a high specific energy of 36.3 Wh kg^{-1} at a power density of 800.2 W kg^{-1}. By integrating the high capacity of pseudocapacitive CBC-N@LDH composite and highly conductive nitrogen-doped carbon nanofibers, the design in this work puts forward a promising approach for exploiting next-generation high-performance energy storage devices.

4. Experimental Section

Materials: The bacterial cellulose pellicles (30 × 40 cm^2) were purchased from Hainan Yide Food Co. Ltd. Aniline (ANI), ammonium persulfate [$(NH_4)_2S_2O_8$, APS], cobalt nitrate hexahydrate [$Co(NO_3)_2{\cdot}6H_2O$], hexamethylenetetramine (HMT), sodium hydroxide (NaOH), hydrochloric acid (HCl) and *N,N*-dimethylformamide (DMF) were all purchased from Sinopharm Chemical Reagent Co. Nickel nitrate hexahydrate [$Ni(NO_3)_2{\bullet}6H_2O$] was purchased

from Aladdin Chemical Reagent Co. All chemicals were of analytic grade and used without further purification.

Preparation of CBC-N Nanofibers: CBC-N nanofibers were prepared according to our previous work.[36] Briefly, raw BC pellicles were cut into rectangular slices (4×5 cm^2) to be frozen in liquid nitrogen (–196 °C), and subsequently freeze-dried in a freezer dryer. After adequate immersion in 75 mL HCl solution (1 mol L^{-1}) containing varied concentrations of aniline monomers (0.004 M, 0.04 M, and 0.4 M), the freeze-dried BC slices (100 mg) adsorbed enough aniline because of the strong hydrogen bonds between bacterial cellulose and aniline monomers. The oxidative polymerization of aniline monomers was taken out at an ice-water bath of 0 °C by dropwise adding another 75 mL HCl solution (1 mol L^{-1}) with different amounts of APS (34.2 mg, 342 mg and 3420 mg, respectively) to form polyaniline (PANI). After reacting for 5 h, the product was washed with deionized water for several times to obtain polyaniline coated bacterial cellulose (denoted as BC/PANI) composite membranes. Finally, the freeze-dried BC/PANI hybrid membranes were carbonized under Ar atmosphere at 700 °C for 2 h with a heating rate of 5 °C min^{-1}, and named as CBC-N1, CBC-N2, and CBC-N3 with increasing coverage of PANI, respectively.

Preparation of CBC-N@LDH Composites: The nickel-cobalt layered double hydroxides were synthesized through solution co-deposition (SCD) method as previously reported.[37] In a typical synthesis, 0.4 mmol $Ni(NO_3)_2{\cdot}6H_2O$, 0.8 mmol $Co(NO_3)_2{\cdot}6H_2O$ and 4 mmol HMT were dissolved into a mixed solution of 15 mL ethanol and 15 mL deionized water under stirring to form a transparent pink solution. Then, 20 mg of CBC-N2 nanofiber powder was immersed into the above solution, heated up to 80 °C and kept for 8 h. Finally, the obtained products were washed with distilled water/ethanol for several times, and overnight dried at 70 °C in air, which was named as CBC-N2@LDH-0.4 composite. Furthermore, the loading mass of Ni-Co LDH was controlled by regulating the precursor dosages of Ni^{2+} (i.e., 0.1 and 0.7 mmol $Ni(NO_3)_2{\cdot}6H_2O$) at a fixed molar ratio of 1/2/10 for Ni^{2+}/Co^{2+}/HMT to obtain the corresponding composites, which were denoted as CBC-N2@LDH-0.1 and CBC-N2@LDH-0.7, respectively. In addition, pure Ni-Co LDH powder was prepared via the same step for comparison. The overall synthesis procedure for CBC-N@LDH composites is shown in Figure 1a.

Characterization: Morphology of CBC-N@LDH composites was observed by field-emission scanning electron microscope (FESEM, Ultra 55, Zeiss) at an acceleration voltage of 5 kV and transmission electron microscopy (TEM, JEOL-2010) at an acceleration voltage of 200 kV. The Brunauer-Emmett-Teller (BET) method was utilized to calculate the specific surface area, by using a Belsorp-max surface area detecting instrument (Tristar3000). The pore size distribution was obtained from the adsorption branches of isotherms by Barrett-Joyner-Halenda (BJH) method. Structure of the samples was tested by X-ray diffraction (XRD, X'pert PRO, PANalytical) with Cu Kα radiation ($\lambda = 0.1542$ nm) at an angular speed of 5° min^{-1} (2θ) from 10° to 70° under a voltage of 40 kV and a current of 40 mA. The chemical composition was examined by X-ray photoelectron spectroscopy (XPS) on a RBD upgraded PHI-5000C ESCA system (Perkin Elmer) with Al Kα radiation ($h\nu = 1486.6$ eV). All XPS spectra were corrected according to the C1s line at 284.6 eV, while curve fitting and background subtraction were accomplished using the RBD AugerScan 3.21 software provided by RBD Enterprises. Thermogravimetric analysis (TGA, Pyris 1 TGA, PerkinElmer) was performed in air from 100 °C to 700 °C at a heating rate of 20 °C min^{-1} in order to measure the mass content of Ni-Co LDH in the composites.

Electrochemical Measurements with a Three-Electrode System: Electrochemical measurements were conducted in 6 M KOH aqueous solution on an electrochemical working station (CHI600D, Chenhua Instruments Co. Ltd., Shanghai) with a standard three-electrode setup where Ag/AgCl and Pt wire were used as the reference and counter electrode, respectively. The working electrode was prepared by mixing the produced powder (milled using a quartz mortar), carbon black, and poly(tetrafluoroethylene) in a mass ratio of 80:10:10 to obtain slurry. Then, the slurry was pressed onto the nickel foam current collector and dried at 80 °C for 12 h with a fixed mass loading of the electrode materials at 3 mg. Cyclic voltammograms (CVs) under various scan rates were obtained from –1 to 0 V and 0 to 0.5 V for CBC-N nanofibers and CBC-N@LDH composites, respectively. Galvanostatic charge-discharge (GCD) testing under different current densities was performed between –1 and 0 V, 0 and 0.4 V for CBC-N nanofibers and CBC-N@LDH composites, respectively. The electrochemical impedance spectroscopy (EIS) measurements were conducted by applying an AC voltage in the frequency ranging from 10 mHz to 100 kHz with an amplitude of 5 mV. Specific capacitance of the electrodes can be calculated from galvanostatic charge-discharge curves according to the following equation:

$$C = \frac{I \times \Delta t}{m \times V} \tag{3}$$

where I is the current (A), V is the potential (V), m is the mass of electroactive materials (g), and Δt is the discharge time (s).

Electrochemical Measurements of the Asymmetric Supercapacitors: The asymmetric supercapacitor (ASC) is constructed by using CBC-N2@LDH-0.4 composite as the positive electrode material and CBC-N2 nanofibers as the negative electrode material. The mass ratio of CBC-N2@LDH-0.4 composite to CBC-N2 nanofibers was set as 1.7 according to their specific capacitances obtained from the three-electrode system, which can be estimated from the following equation: where C is the specific capacitance (F g^{-1}), V is the potential (V), and m is the mass of the electrode (g).

Galvanostatic charge–discharge curves were measured at different current densities varied from 1 to 10 A g^{-1} to evaluate the energy density and power density of the asymmetric supercapacitor using the following Equations (4) and (5):

$$E = \frac{1}{2} \times C \times V^2 \tag{4}$$

$$P = \frac{E}{\Delta t} \tag{5}$$

$$\frac{m_+}{m_-} = \frac{C_- \times V_-}{C_+ \times V_+} \tag{6}$$

where C is the specific capacitance (F g^{-1}), V is the potential (V), Δt is the discharge time (s), E is the energy density (Wh kg^{-1}) and P is the power density (W kg^{-1}).

Supporting Information

Supporting Information is available from the Wiley Online Library or from the author.

Acknowledgements

The authors are grateful for the financial support from the National Natural Science Foundation of China (51125011, 51373037, 51433001).

[1] Y. Zhao, J. Liu, Y. Hu, H. H. Cheng, C. G. Hu, C. C. Jiang, L. Jiang, L. Jiang, A. Y. Cao, L. T. Qu, *Adv. Mater.* **2013**, *25*, 591.
[2] H. C. Chen, J. J. Jiang, L. Zhang, Y. D. Zhao, D. Q. Guo, Y. J. Ruan, D. D. Xia, *ChemPlusChem* **2015**, *80*, 181.
[3] H. L. Wang, H. S. Casalongue, Y. Y. Liang, H. J. Dai, *J. Am. Chem. Soc.* **2010**, *132*, 7472.
[4] X. L. Wu, L. L. Jiang, C. L. Long, T. Wei, Z. J. Fan, *Adv. Funct. Mater.* **2015**, *25*, 1648.
[5] F. H. Xu, X. M. Lv, M. H. Miao, *Small* **2015**, *11*, 854.
[6] Y. F. Song, J. Yang, K. Wang, S. Haller, Y. G. Wang, C. X. Wang, *Carbon* **2016**, *96*, 955.
[7] M. K. Liu, W. W. Tjiu, J. S. Pan, C. Zhang, W. Gao, T. X. Liu, *Nanoscale* **2014**, *6*, 4233.
[8] W. Wang, W. Y. Liu, Y. X. Zeng, Y. Han, M. H. Yu, X. H. Lu, Y. X. Tong, *Adv. Mater.* **2015**, *27*, 3572.
[9] J. W. Zhao, J. L. Chen, S. M. Xu, M. F. Shao, Q. Zhang, F. Wei, J. Ma, M. Wei, D. G. Evans, X. Duan, *Adv. Funct. Mater.* **2014**, *24*, 2938.
[10] G. Q. Zhang, H. B. Wu, H. E. Hoster, M. B. Chan-Park, X. W. Lou, *Energy Environ. Sci.* **2012**, *5*, 9453.
[11] H. Chen, L. F. Hu, M. Chen, Y. Yan, L. M. Wu, *Adv. Funct. Mater.* **2014**, *24*, 934.
[12] J. Bao, X. D. Zhang, B. Fan, J. J. Zhang, M. Zhou, W. L. Yang, X. Hu, H. Wang, B. C. Pan, Y. Xie, *Angew. Chem.-Int. Ed.* **2015**, *54*, 7399.
[13] J. H. Zhu, J. Jiang, Z. P. Sun, J. S. Luo, Z. X. Fan, X. T. Huang, H. Zhang, T. Yu, *Small* **2014**, *14*, 2937.
[14] F. L. Lai, Y. P. Huang, Y. E. Miao, T. X. Liu, *Electrochim. Acta* **2015**, *174*, 456.
[15] F. Y. Ning, M. F. Shao, C. L. Zhang, S. M. Xu, M. Wei, X. Duan, *Nano Energy* **2014**, *7*, 134.
[16] X. Xu, H. Zhou, S. J. Ding, J. Li, B. B. Li, D. M. Yu, *J. Power Sources* **2014**, *267*, 641.
[17] Y. F. Tang, Y. Y. Liu, S. X. Yu, W. C. Guo, S. C. Mu, H. C. Wang, Y. F. Zhao, L. Hou, Y. Q. Fan, F. M. Gao, *Electrochim. Acta* **2015**, *161*, 279.
[18] R. R. Salunkhe, K. Jang, S. W. Lee, S. Yu, H. Ahn, *J. Mater. Chem.* **2012**, *22*, 21630.
[19] X. Wang, W. S. Liu, X. H. Lu, P. S. Lee, *J. Mater. Chem.* **2012**, *22*, 23114.
[20] T. Yan, R. Y. Li, Z. Li, *Mater. Res. Bull.* **2014**, *51*, 97.
[21] L. Huang, D. C. Chen, Y. Ding, S. Feng, Z. L. Wang, M. L. Liu, *Nano Lett.* **2013**, *13*, 3135.
[22] M. F. Warsi, I. Shakir, M. Shahid, M. Sarfrazb, M. Nadeemd, Z. A. Gilani, *Electrochim. Acta* **2014**, *135*, 513.
[23] G. Q. Zhang, X. W. Lou, *Sci. Rep.* **2013**, *3*, 1470.
[24] A. Aboagye, H. Elbohy, A. D. Kelkar, Q. Qian, J. T. Zai, X. F. Qian, L. F. Zhang, *Nano Energy* **2015**, *11*, 550.
[25] Y. E. Miao, J. J. Yan, Y. P. Huang, W. Fan, T. X. Liu, *RSC Adv.* **2015**, *5*, 26189.
[26] Z. Y. Fan, J. Liang, W. Yu, S. J. Ding, S. D. Chen, G. Yang, Y. L. Wang, Y. X. Xi, K. Xi, R. V. Kumar, *Nano Energy* **2015**, *16*, 152.
[27] C. T. Chen, Y. Huang, C. L. Zhu, Y. Nie, J. Z. Yang, D. P. Sun, *Chin. J. Polym. Sci.* **2014**, *32*, 439.
[28] F. L. Lai, Y. E. Miao, L. Z. Zuo, Y. F. Zhang, T. X. Liu, *ChemNanoMat* **2016**, *2*, 212.
[29] C. L. Long, D. P. Qi, T. Wei, J. Yan, L. L. Jiang, Z. J. Fan, *Adv. Funct. Mater.* **2014**, *24*, 3953.
[30] W. Czaja, A. Krystynowicz, S. Bielecki, R. Brown, *Biomaterials* **2006**, *27*, 145.
[31] L. F. Chen, Z. H. Huang, H. W. Liang, H. L. Gao, S. H. Yu, *Adv. Funct. Mater.* **2014**, *24*, 5104.
[32] W. D. Yu, W. L. Lin, X. F. Shao, Z. X. Hu, R. C. Li, D. S. Yuan, *J. Power Sources* **2014**, *272*, 137.
[33] Z. Y. Wu, H. W. Liang, C. Li, B. C. Hu, Q. Wang, J. F. Chen, S. H. Yu, *Nano Res.* **2014**, *7*, 1861.
[34] Q. W. Qian, J. Y. Zhu, Y. Zhang, X. Wu, F. Yan, *Small* **2015**, *11*, 4959.
[35] L. F. Chen, Z. H. Huang, H. W. Liang, W. T. Yao, Z. Y. Yu, S. H. Yu, *Energy Environ. Sci.* **2013**, *6*, 3331.
[36] F. L. Lai, Y. E. Miao, Y. P. Huang, Y. F. Zhang, T. X. Liu, *ACS Appl. Mater. Interfaces* **2016**, *8*, 3558.
[37] F. L. Lai, Y. E. Miao, Y. P. Huang, T. S. Chung, T. X. Liu, *J. Phys. Chem. C* **2015**, *119*, 13442.
[38] W. L. Hu, S. Y. Chen, Z. H. Yang, L. T. Liu, H. P. Wang, *J. Phys. Chem. B* **2011**, *115*, 8453.
[39] H. G. O. Barud, H. D. S. Barud, M. Cavicchioli, T. S. Amaral, O. B. Oliveira, D. M. Santos, A. L. D. A. Petersen, F. Celes, V. M. Borges, C. Oliveira, *Carbohydr. Polym.* **2015**, *128*, 41.
[40] W. Wang, Y. Sun, B. Liu, S. G. Wang, M. H. Gao, *Carbon* **2015**, *91*, 56.
[41] H. W. Liang, Z. Y. Wu, L. F. Chen, C. Li, S. H. Yu, *Nano Energy* **2015**, *11*, 366.
[42] R. Z. Ma, J. B. Liang, K. Takada, T. Sasaki, *J. Am. Chem. Soc.* **2011**, *3*, 613.
[43] Y. T. Hu, H. J. Liu, Q. Q. Ke, J. Wang, *J. Mater. Chem. A* **2014**, *2*, 11753.
[44] Y. F. Zhao, W. Ran, J. He, Y. Z. Huang, Z. F. Liu, W. Liu, Y. F. Tang, L. Zhang, D. W. Gao, F. M. Gao, *Small* **2015**, *11*, 1310.
[45] R. R. Salunkhe, Y. Kamachi, N. L. Torad, S. M. Hwang, Z. Q. Sun, S. X. Dou, J. H. Kim, Y. Yamauchi, *J. Mater. Chem. A* **2014**, *2*, 19848.
[46] Z. R. Chang, Y. J. Zhao, Y. C. Ding, *J. Power Sources* **1999**, *77*, 69.
[47] Y. Bai, W. Q. Wang, R. R. Wang, J. Sun, L. Gao, *J. Mater. Chem. A* **2015**, *3*, 12530.
[48] J. C. Chen, C. T. Hsu, C. C. Hu, *J. Power Sources* **2014**, *253*, 205.
[49] J. Zhang, J. P. Cheng, M. Li, L. Liu, F. Liu, X. B. Zhang, *J. Electroanal. Chem.* **2015**, *743*, 38.
[50] W. Xu, A. Sumboja, L. M. F. Lin, J. Yan, P. S. Lee, *Nanoscale* **2012**, *4*, 7266.

Received: February 6, 2016
Revised: March 14, 2016
Published online: May 2, 2016